Flavin-Helicene Amphiphilic Hybrids: Synthesis, Characterization, and Preparation of Surface-Supported Films

Martin Jakubec, David Novak, Martina Zatloukalova, Ivana Cisarova, Radek Cibulka, Ludovic Favereau, Jeanne Crassous, Adrianna Cytryniak, Renata Bilewicz, Jan Hrbac, et al.

Flavin-helicene amphiphilic hybrid synthesis, characterization, and preparation of solid surface supported films

Martin Jakubec,[1,*] David Novák,[2,*] Martina Zatloukalová,[2] Ivana Císařová,[3] Radek Cibulka,[4] Ludovic Favereau,[5] Jeanne Crassous,[5] Adrianna Cytryniak,[6] Renata Bilewicz,[6] Jan Hrbáč,[7] Jan Storch,[1] Jaroslav Žádný,[1,**] Jan Vacek[2,***]

[1] Institute of Chemical Process Fundamentals of the Czech Academy of Sciences, v.v.i., Rozvojová 135, 165 02 Prague 6, Czech Republic

[2] Department of Medical Chemistry and Biochemistry, Faculty of Medicine and Dentistry, Palacký University, Hněvotínská 3, 775 15 Olomouc, Czech Republic

[3] Department of Inorganic Chemistry, Faculty of Science, Charles University in Prague, Hlavova 2030, 128 40 Prague 2, Czech Republic

[4] Department of Organic Chemistry, University of Chemistry and Technology, Technická 5, 166 28 Prague, Czech Republic

[5] Univ Rennes, CNRS, ISCR-UMR 6226, Campus de Beaulieu, 35042 Rennes Cedex, France

[6] Faculty of Chemistry, University of Warsaw, Pasteura 1, Warsaw, 02-093, Poland

[7] Institute of Chemistry, Masaryk University, Kamenice 5, Brno, 725 00, Czech Republic

*) Both authors contributed equally.

Corresponding authors: **) J. Žádný, responsible for synthetic work, ***) J. Vacek, responsible for characterization studies

ABSTRACT

The tuning of helicene properties *via* conjugation with other functional moieties could result in new chiral hybrid molecules with unique photophysical and chiroptical properties. Here we focused on the preparation and structural characterization of flavo[7]helicene **1** (flavin-[7]helicene conjugate), which was subsequently characterized at the molecular level in either

an aqueous environment or an organic phase, at the supramolecular level in the form of polymeric layers, and also embedded in a lipidic mesophase environment to study the resulting properties of such a hybrid relative to its parent molecules. The flavin benzo[*g*]pteridin-2,4-dione (isoalloxazine) was selected for conjugation because of its photoactivity and reversible redox behavior. Compound **1** was prepared from 2-nitroso[6]helicene and 6-methylamino-3-methyluracil, and characterized using common structural and spectroscopic tools: circular dichroism (CD), circularly polarized luminescence (CPL) spectroscopy, cyclic voltammetry (CV), and DFT quantum calculations. In addition, the loading of **1** into a 1-monoolein cubic phase is to the best of our knowledge the first example of a helicene-based transparent and soft material.

Keywords: helicene, flavin, lipidic cubic phase, redox behavior, thin layers

INTRODUCTION

Helicenes are a class of polyaromatic compounds with *ortho*-fused benzene rings that have been studied for the past few decades due to their particularly intense (chir)optical and electronic properties,[1] which demonstrate their potential for applications in optoelectronics and other materials sciences. Along with circular dichroism, helicenes were found to exhibit circularly polarized photoluminescence or electrochemiluminescence.[2] In addition to the study of helicenes as monomers in solution, they were also applied in a solid phase as semiconductors,[3] electrosynthesized polymers,[3] or generally as active layers in electronic devices.[4]

The applicability of helicenes can be further widened by modifying their structure, which results in a modulation of their properties, such as chiroptical and redox behavior, or improvement of their solubility (for an overview see, ref.[5]). The most typical ways to attach the functional group(s) include their introduction directly onto the helical skeleton or connection *via* a linker (**Scheme 1A**). This can be commonly achieved by electrophilic substitution, oxidation, C-H activation, or by transformations of reactive groups bound to helicenes.[6] The direct connection of the functional group is typically accompanied by electron redistribution along the π-electron system with a subsequent change in helicene properties, while the use of linkers allows the functionality of the attached group to be kept separate from the helicene part.[6] Similarly, building more complex helicene-based structures (**Scheme 1B**), such as oligomers/polymers or self-assembled systems can result in a significant change in their physico-chemical properties through conjugation, depending on the character of the linker or solvent.[7] The most dramatic changes in electronic structure can be expected by the introduction of heteroatom(s) into a

helicene backbone, giving rise to heterohelicenes[5, 8] (**Scheme 1C**). An extension of the existing π-electron system (**Scheme 1D**) by various structural motifs (*e.g.* ref.[6, 9]) can also lead to charge redistribution, and thus impact the final properties of the molecule and of the resulting polymeric or supramolecular assembly.

Scheme 1. (A) Direct and *via* linker functionalization. **(B)** Oligo- and polymerization approaches. **(C)** Introduction of heteroatom into skeleton. **(D)** Functionalization with π-extended systems.

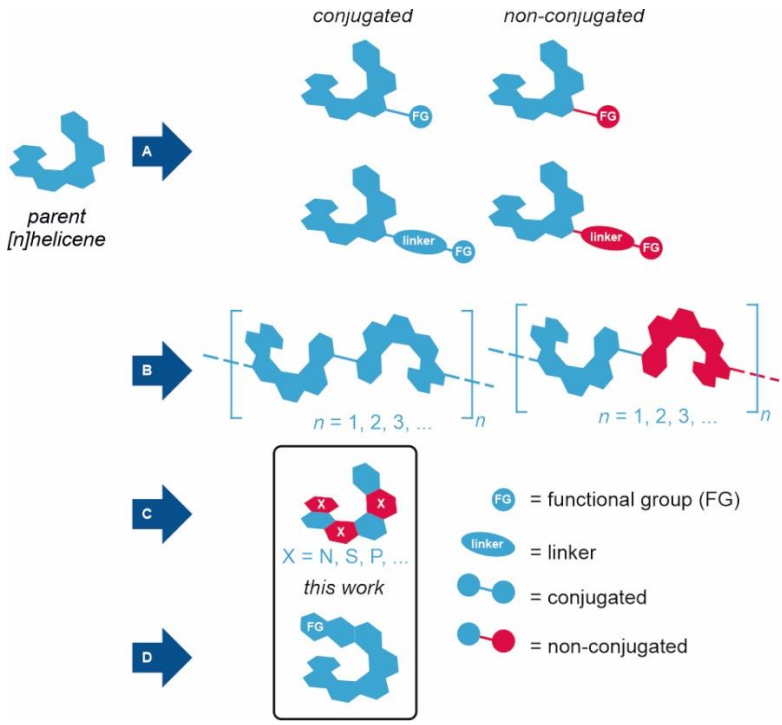

Of the wide spectrum of possible functional groups that can be attached to the helical skeleton, those which originate from natural products or compounds of biological relevance are very rare.[1] Here, we chose a flavin (isoalloxazine) for incorporation into helicene. This compound is known to have properties that would be an attractive addition to those of helicenes, especially improving solubility in polar solvents, reversible redox behavior, and changing electronic and optical properties or its catalytic activity.[10]

Based on the combination of synthetic approaches mentioned above (**Schemes 1C and 1D**), we prepared a new flavin-helicene hybrid, here denoted as flavo[7]helicene (**1**) (see **Scheme 2**) to study the impact of flavin substitution on the physico-chemical properties of helicene. It was first investigated by common structural tools and spectroscopic techniques. Secondly, the impact of the environment on the resulting properties of compound **1** was studied, *i.e.* aqueous solution, organic solvents, a lipidic cubic phase, polymeric thin film, and solid state. Moreover,

the utilization of lipidic cubic phases (LCPs) for the loading of an inherently chiral molecule is presented here for the first time. The properties of the mesophase were characterized by small-angle X-ray scattering (SAXS) and cyclic voltammetry.

RESULTS AND DISCUSSION

Synthesis of 1 and separation of its enantiomers. Despite the fact that the synthesis of a similar flavin-helicene hybrid structure was published recently,[9] this study of targeted compound **1** (**Scheme 2**) is not only focused on its synthesis, but also presents a detailed study of its properties. In this case, the flavin part was directly conjugated to the periphery of the starting helicene, extending its π-conjugated system.

Scheme 2. Synthesis of compound **1**. The flavin part is red, the part forming the helicene is highlighted in light blue.

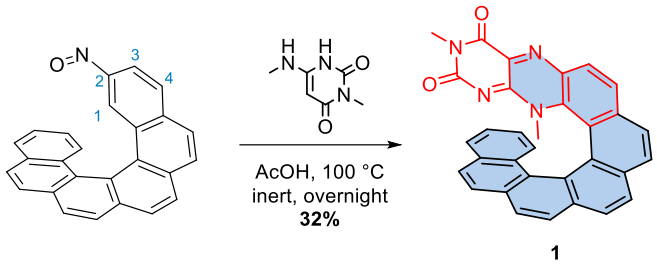

1

The synthesis of compound **1** was designed by following a general approach for forming an isoalloxazine moiety[11] from aminouracil and nitrosoaromates. Accordingly, 2-nitroso[6]helicene[12] was mixed with 6-methylamino-3-methyl uracil in carefully degassed glacial acetic acid under an inert atmosphere and heated to 100 °C overnight (**Scheme 2**). Product **1** was isolated using column chromatography as a magenta solid in a 32% yield (for details see Experimental section). Despite the presence of two possible positions (C1 and C3, see the numbering in **Scheme 2**), where the cyclization may occur, only the product of cyclization at position C1 of the helicene was observed. This happened despite the increased steric hindrance at the C1 position, and consequently led to the extension of the helical part of the molecule to seven *ortho*-fused rings (in **Scheme 2** in light blue). The structure was confirmed by X-ray analysis (for details, see the section on X-ray crystallography). The racemic **1** was subsequently resolved to (*P*)- and (*M*)-enantiomers using semi-preparative HPLC with the chiral stationary phase (for details, see Experimental section and Supplementary Information).

In compound **1**, a significant interplay of the helicenes' chirality and flavin functionality can be expected as a consequence of the structural change. Among them, reversible redox activity is

one of the most distinctive, thus the properties of compound **1** in both redox states (**1** and **1-H$_2$**) were first studied by *in silico* calculations.

DFT study. The introduction of flavin as a known reversible redox-active moiety into helicene **1** allowed for a more detailed electronic structure investigation. Both **1** and its expected two-electron-reduced form **1-H$_2$** were chosen for DFT calculations (**Scheme 3**) analogous to those for known redox states of other flavin-derivatives. All calculations were performed at the B3LYP/6-31G(d) level of theory.

Scheme 3. (**A**) Electrostatic potentials for **1** and **1-H$_2$** in the range from −0.03 (red) to +0.03 (blue). (**B**) HOMO (bottom) and LUMO (up) of **1** and **1-H$_2$** front (left) and side (right) view. For simplicity, only the (*P*)-enantiomer is depicted.

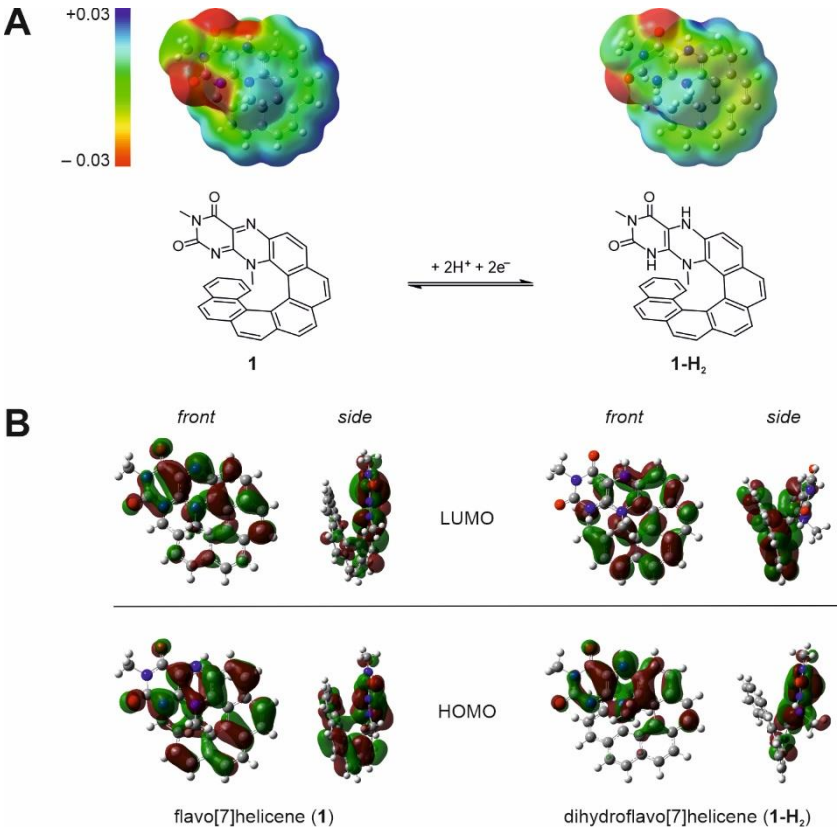

There are strong differences between the electrostatic potentials of **1** and **1-H$_2$**, where the parent 'oxidized' form is more negatively charged at the flavin moiety (**Scheme 3A**). Strong electron delocalization of HOMO was found for **1** (similarly to [7]helicene **2**; for details see Supporting Information), whereas for the **1-H$_2$** redox state, this orbital was predominantly localized on or around the flavin moiety. For LUMO orbitals, the observed trend was the opposite (**Scheme**

3B). The values –5.78 eV (HOMO) and –2.79 eV (LUMO) were found for **1**, whereas for **1-H$_2$** shifts to –4.72 eV (HOMO) and –1.67 eV (LUMO) were observed, respectively. While the HOMO-LUMO gap was almost independent of the redox state of the flavin part, the HOMO and LUMO energy levels increased by approx. 1 eV upon reduction. In comparison with unsubstituted heptahelicene **2**, the HOMO energy level of **1** increased negligibly, whereas the LUMO energy level dropped substantially, resulting in a significant decrease in the HOMO-LUMO energy gap by approx. 0.9 eV (**Table 1**). Similarly, the same trend of HOMO-LUMO energy gap decrease was found in both redox states of flavin **3** and **3-H$_2$**, relative to **1** (the structures **1-3** and **1-H$_2$, 3-H$_2$** are depicted below **Table 1**).

Table 1. HOMO, LUMO, and their energy gaps for **1**, **1-H$_2$**, [7]helicene **2**, and flavin **3** and **3-H$_2$** respectively, calculated by DFT using the B3LYP/6-31G(d) level of theory.

Energy (eV)	**1** (ox.)	**1-H$_2$** (red.)	**2**	**3** (ox.)	**3-H$_2$** (red.)
LUMO	-2.79	-1.67	-1.49	-2.94	-0.74
HOMO	-5.78	-4.72	-5.36	-6.44	-4.59
HOMO-LUMO gap	2.99	3.04	3.86	3.50	3.85

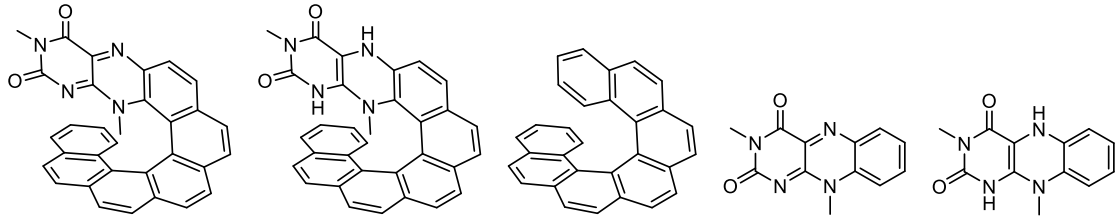

1 **1-H$_2$** **2** **3** **3-H$_2$**

In order to evaluate the calculations, the synthesis of **1-H$_2$** was attempted using the hydrogen-promoted reduction of **1**, however, a fast re-oxidation occurred (see details in Experimental section), which is also common with other flavin derivatives.[10] Thorough experimental studies of the reduced form **1-H$_2$** were therefore difficult. Nevertheless, the stabilization of **1-H$_2$** by the application of potential is mentioned in the Electrochemical studies section. In addition to theoretical studies, compound **1** was investigated using various techniques mentioned in the sections below, either in solution or upon loading into LCPs.

Preparation of lipid mesophase. LCPs are transparent and soft materials with highly-ordered topology containing aqueous nanochannels that can be used for the accumulation of molecules of biological, medical and technological relevance.[13] Analytical chemistry, biochemistry, and materials science are the main research areas where LCPs are currently applied.[13a, 14] Here the LCP was used for loading enantiopure **1**, resulting in a new material exhibiting optical activity (see the details below). The lipid cubic mesophase structure consists of a highly curved

continuous lipid bilayer that separates interpenetrating, nonintersecting aqueous channels, and it can coexist at thermodynamic equilibrium with excess water. Flavo[7]helicene **1** was used for its amphiphilic character, and was expected to incorporate easily into the lipidic bilayer walls with the polar flavin part exposed to the aqueous medium. LCPs containing optically pure **1** (here denoted as (*P*)/(*M*)-**1**@LCPs) were prepared upon dissolution in molten 1-monoolein (MO) phase and water (for details, see Experimental part and Supplementary Information). Small-angle X-ray scattering (SAXS) analysis was used to confirm the symmetry and structural parameters of LCP with and without incorporated enantiomers of **1** at a ratio of 59.8/0.2/40 (%, *w*/*w*) for MO/**1**/water and 60/40 (%, *w*/*w*) for MO/water respectively (**Figure 1**).

Figure 1. SAXS profiles of 1-monoolein-based lipid cubic phase (LCP) without (black) or with incorporated (*P*)-**1** ((*P*)-**1**@LCP in red) and (*M*)-**1** ((*M*)-**1**@LCP in blue).

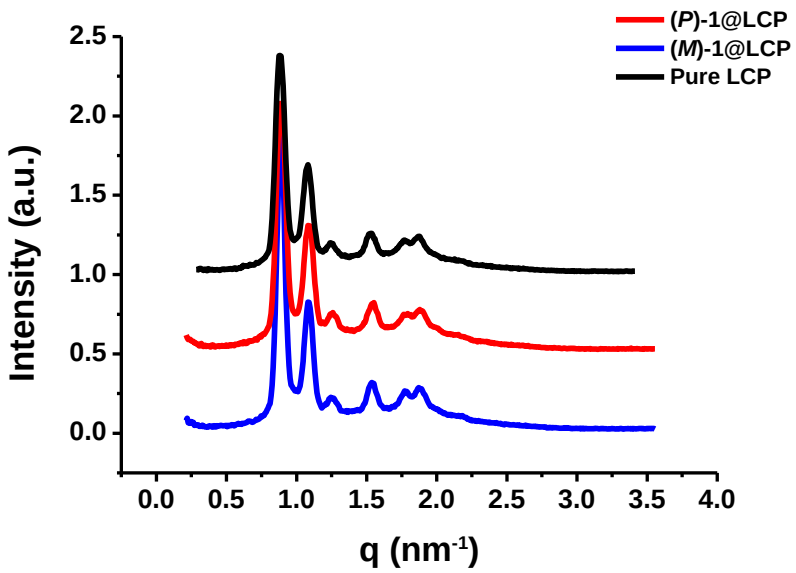

The 1D diffraction pattern of the studied LCPs showed reflections in the ratios √2, √3, √4, √6, √8, and √9, characteristic for a cubic phase with *Pn3m* symmetry.[15] Only negligible changes in the parameters such as lattice parameter *a*, lipid chain length, or channel width show that the incorporation of enantiomers of **1** did not change the internal structure of the LCPs (**Table 2**), however its incorporation was easily visually detectable and consequently confirmed by UV and other techniques. The resulting **1**@LCPs formed a transparent and soft helicene-based material, which can be immobilized onto electrodes or solid supports in general.

Table 2. Structural parameters of LCPs with or without incorporated enantiomers of **1**.

LCPs	Composition MO[a]/**1**/water (w/w) %	Phase symmetry	Lattice parameter *a* (nm)	Lipid length *l* (nm)	Channel width *d* (nm)
LCP	60/0/40	*Pn3m*	10.07	1.68	4.53
(*M*)-**1**@LCP	59.8/0.2/40	*Pn3m*	10.01	1.67	4.5
(*P*)-**1**@LCP	59.8/0.2/40	*Pn3m*	9.99	1.66	4.49

[a]) MO = monoolein

Electrochemical studies. Compound **1** or **1**@LCPs were further studied in solution in both polar and non-polar solvents or upon deposition onto the electrode surface. Cyclic voltammetry (CV) was performed using a glassy carbon electrode (GCE). For in-solution experiments, **1** was dissolved in DMSO and then diluted in the supporting electrolyte; an aqueous buffer or DCM/TBAP (tetrabutylammonium perchlorate), depending on the experimental setup. The solubility (up to 50 μM, confirmed by UV-vis measurement) of compound **1** in water was found to be unusually high in contrast to most helicenes, and allowed for the measurement of CV in aqueous electrolytes. All electrochemical experiments performed in aqueous solution were evaluated in Britton-Robinson buffer at pH 7.4 for both (*P*)- and (*M*)-stereomers of **1**, and were found to be identical as expected, so all CVs in the following part are depicted for (*M*)-**1** or (*M*)-**1**@LCP.

In a single CV scan, a flavin redox couple was observed at potentials around –0.35 V (*vs.* Ag/AgCl/3M KCl), in agreement with literature data referring to the two-electron process in an aqueous medium[16] (**Figure 2A**). In the anodic part of the full CV record, a peak at +1.4 V was attributed to irreversible oxidation of the helicene moiety, resulting in the formation of radical species and a subsequent formation of a deposit on the electrode surface.[17] This allowed us to modify the electrode surface with the helicene-based polymer. Redox cycling *in situ* (in solution containing **1**) at the potential region of the flavin redox couple is shown in **Figure 2B**. Redox cycling of flavin could also be observed after the formation of the deposit using the *ex-situ* approach performed in pure supporting electrolyte (**Figure 2C**). In the aqueous buffer solution, the flavin moiety redox process at ca. -0.4V is quasi-reversible and affected by adsorption, as seen by the symmetrical shape and small separation of the voltammetric peaks. This observation is in agreement with CV theory[18] for electrode processes accompanied by adsorption onto the electrode surface. See Supporting Information for the corresponding I_p *vs. scan rate* plots. Similarly to chemical reduction, **1-H$_2$** was unstable and observable only when a potential lower than -0.4 V was applied.

Figure 2. (A) Cyclic voltammograms of 50 µM (*P*)-**1** (in red) and (*M*)-**1** (in blue) at glassy carbon electrode in aqueous electrolyte. CV records (5 scans) of the (*M*)-enantiomer (in blue) **(B)** *in situ* and **(C)** *ex situ* performed after one full CV scan (resulting in the polymer) under the same conditions as shown in panel **A**.

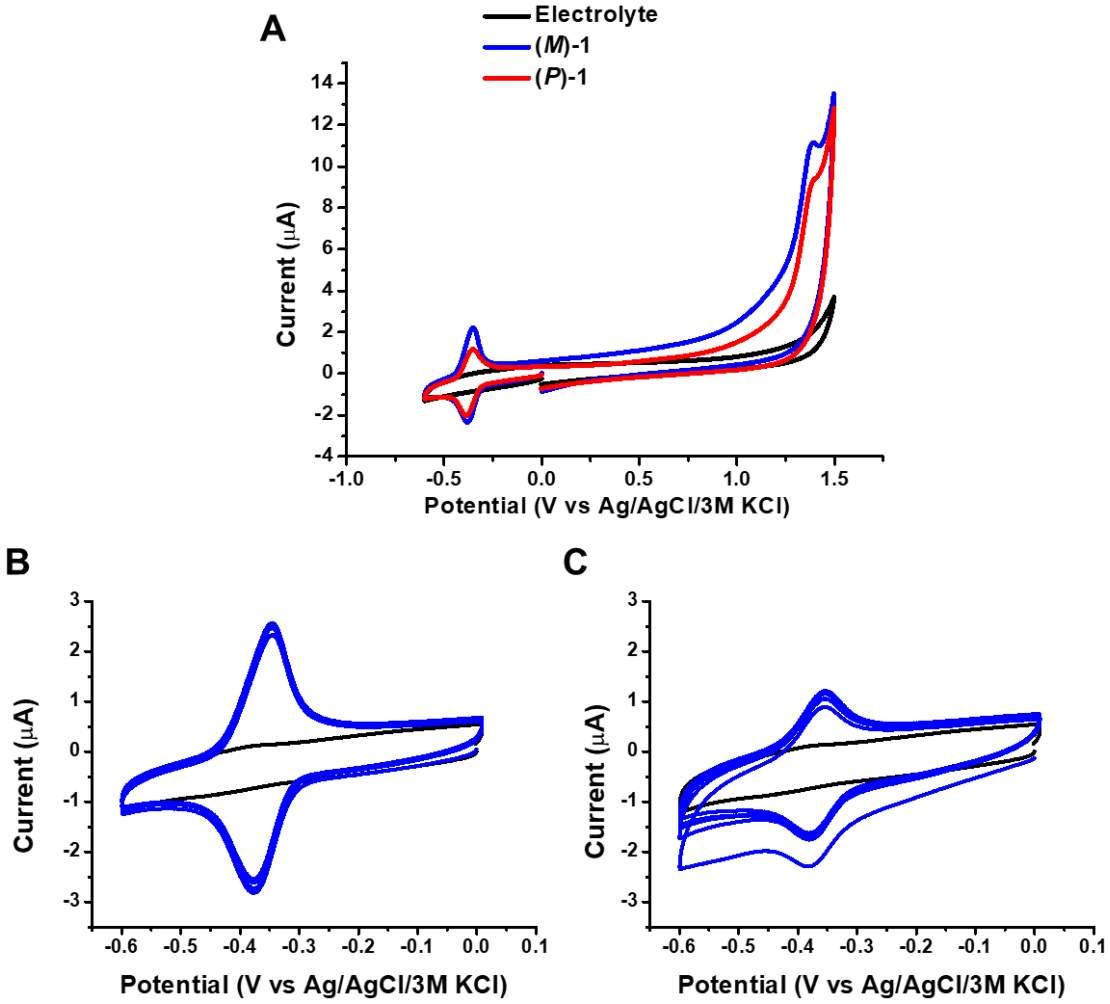

Similarly to the electrochemical behavior in an aqueous environment, the separate processes of flavin and helicene redox transitions could be observed in non-aqueous environments (**Figure 3**). In the ACN/TBAP electrolyte, the helicene moiety provides an oxidation peak with an onset at ca. +1.5 V *vs.* Ag/AgCl, and a reduction peak starting at ca. –2 V. In DCM/TBAP, the helicene oxidation peak is only partly visible, while the helicene reduction peak cannot be observed at all due to the limited potential window of the DCM electrolyte (not shown). However, the redox behavior of the flavin moiety markedly differs from that observed in the aqueous environment. In cyclic voltammograms of **1**, recorded in both ACN and DCM, there are two reversible and separated pairs of peaks, both diffusion-controlled, in contrast to the aqueous environment, where a single surface-confined redox pair is observed, and in the LCP phase, in which there is a single but diffusion-controlled pair of CV peaks (see below). Similar

behavior has been observed for electron-deficient simple flavins in non-aqueous systems, which was explained by two consecutive reversible redox processes.[19] To confirm the assignment of the above redox transitions, the cyclic voltammogram of dimethylisoalloxazine **3** was also recorded and found to be virtually identical to that of **1**.

Figure 3. Cyclic voltammograms of **1** in nonaqueous environments. An experiment with an extended potential scale was performed with *rac*-**1** (in magenta) in ACN/0.1 M TBAP, the background voltammogram (in black) is included for comparison. CVs of (*M*)-**1** (in blue), (*P*)-**1** (in red) and **3** (in green) were obtained in DCM/0.1 M TBAP. In all voltammograms, the potential was scanned in the negative direction, starting at 0 V *vs.* the reference electrode at a scan rate of 0.1V/s.

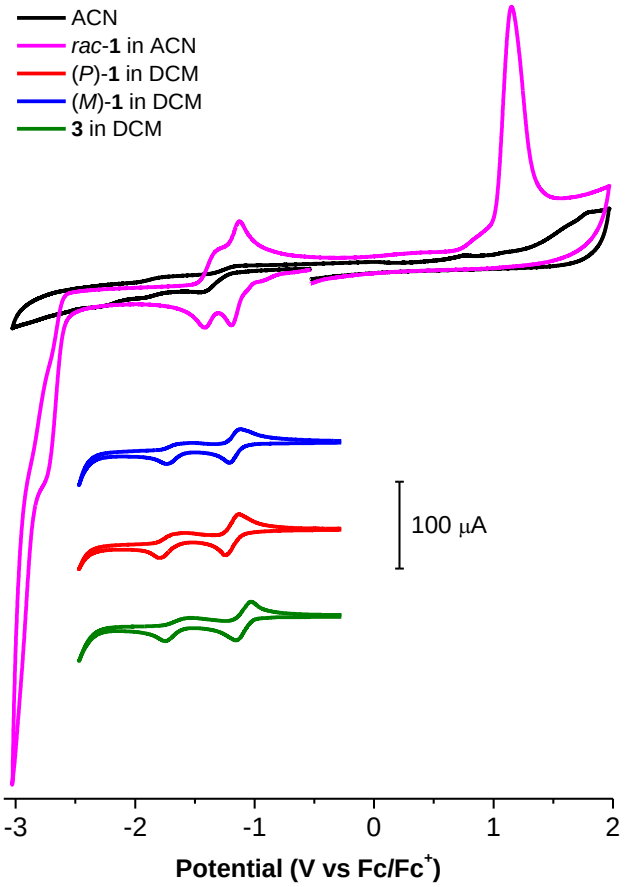

The samples of (*P*)/(*M*)-**1**@LCPs were also studied using CV (**Figure 4A**, for sample preparation, see Supporting Information). As mentioned above, in an LCP phase film the process proceeds in a single $2e^-$ step and is diffusion controlled.[20] The peak currents of the single pair of voltammetric peaks increase linearly with the square root of scan rate, as shown in Supporting Information. The flavin redox couple appears under *ex-situ* conditions at similar potentials as was found in in-solution experiments, *c.f.* **Figures 2** and **4B**. In contrast, the

oxidation peak of the helicene moiety at around +1.4 V was suppressed in a cubic phase embedded with **1**, which indicates that the lipophilic helicene part of the molecule was integrated into LCP lipid bilayers and not in the aqueous channels, which shifted the oxidation to larger overpotentials. Thus, **1** can be immobilized in the cubic phase film placed at the electrode surface, the layer is stable in contact with an aqueous solution, and the complications due to the direct adsorption of **1** at the electrode surface are eliminated. Also, the current corresponding to helicene redox transitions at positive potentials, which lead to polymer formation in the aqueous solution at the bare electrode, is decreased.

Figure 4. (A) Full CV of (*M*)-**1**@LCP (in blue) after its immobilization onto glassy carbon electrode. Inset: the image of (*M*)-**1**@LCP and (*P*)-**1**@LCP (for more details, see Supplementary Information). **(B)** Redox cycling of the same sample as in panel **A**, after cycling to +1.5 V, in pure supporting electrolyte.

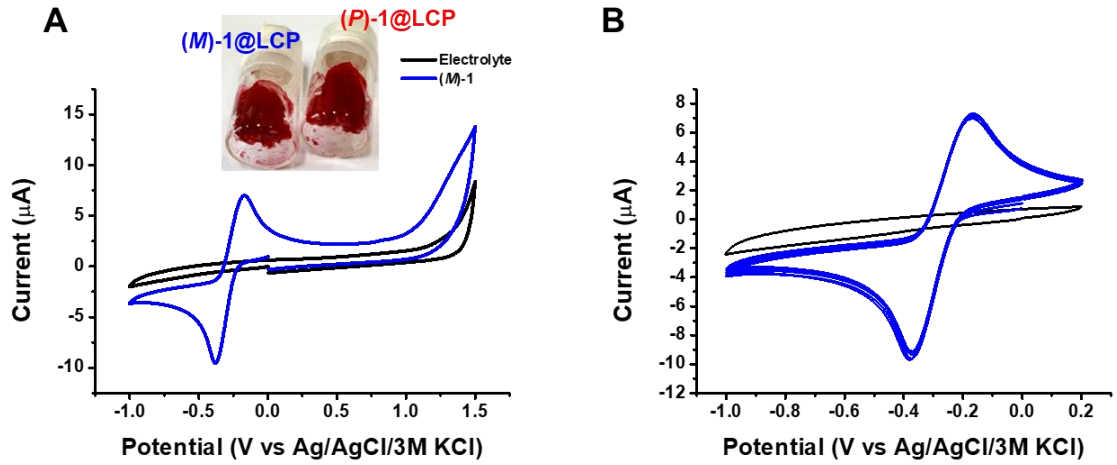

Photophysical and chiroptical properties. In order to evaluate the optical properties of **1**, absorption and emission spectra were measured as well as circular dichroism and CP luminescence. The UV-vis absorption spectrum of **1** was significantly red-shifted compared to unsubstituted helicene **2** (*cf.* [21]). The spectrum of **1** in DCM (c ~10^{-4} M) exhibits several intense bands ($\varepsilon > 25\times10^3$ M^{-1} cm^{-1}) between 230-300 nm, an intense band at 330 nm ($\varepsilon > 18\times10^3$ M^{-1} cm^{-1}) accompanied by a shoulder at 350 nm ($\varepsilon > 9\times10^3$ M^{-1} cm^{-1}), together with a set of less intense bands between 390 ($\varepsilon > 4\times10^3$ M^{-1} cm^{-1}) and 500 nm ($\varepsilon \sim 4\times10^3$ M^{-1} cm^{-1}) (**Figure 5A**). Similar UV spectra were obtained in Britton-Robinson buffer at pH = 7.4 (**Figure 5C**), and are in accordance with theoretically calculated absorption bands (see Supporting Information). This also allowed for the experimental determination of the optical HOMO-LUMO gap (ΔE_{opt} = 1.90 V, see Supporting Information).

Figure 5. (A) UV-vis and **(B)** CD spectra of ~ 10^{-4} M (*P*)-**1** (red curves) and (*M*)-**1** (blue curves) in DCM. **(C)** UV-vis and **(D)** CD spectra of 50 µM (*P*)-**1** and (*M*)-**1** in Britton-Robinson buffer pH 7.4. **(E)** UV-Vis and **(F)** CD spectra of (*P*)-**1**@LCP and (*M*)-**1**@LCP (0.5 mg/ml). **1**@LCPspectra were collected from 300 nm, because of interference originating from glass slides; for experimental setup, see Supporting Information.

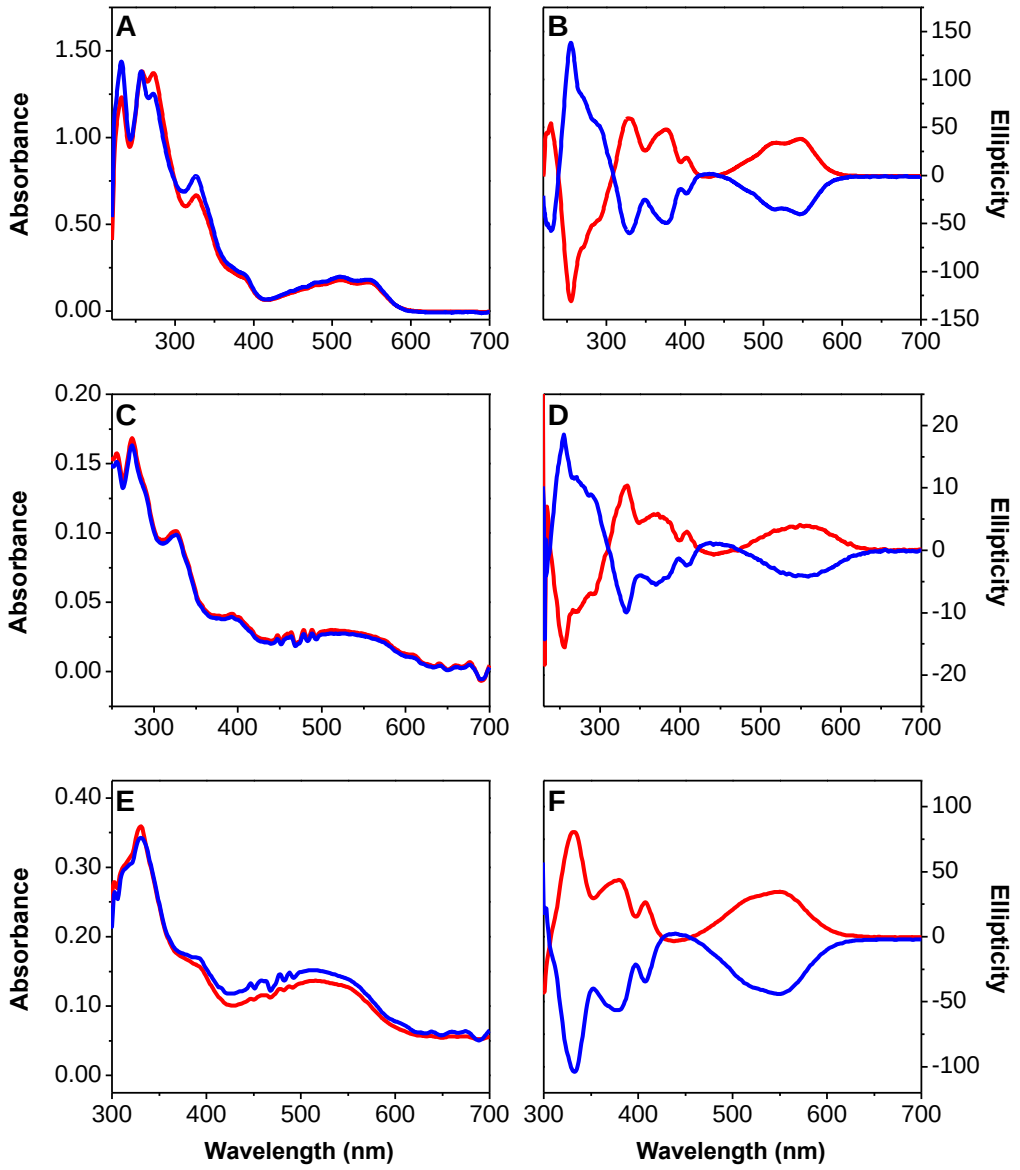

Pure enantiomers of **1** exhibited mirror-imaged electronic circular dichroism (ECD) spectra in DCM and in Britton-Robinson buffer, see **Figures 5B and 5D**. In aqueous solution, the (*P*)-flavo[7]helicene (*P*)-**1** exhibited ECD bands at 230 nm ($\Delta\varepsilon$ = +38 M^{-1} cm^{-1}), 256 ($\Delta\varepsilon$ = −92), 272 ($\Delta\varepsilon$ = −53), 292 ($\Delta\varepsilon$ = −32), 334 ($\Delta\varepsilon$ = +40), 381 ($\Delta\varepsilon$ = +32), 407 (+9), 517 ($\Delta\varepsilon$ = +24), and 551 ($\Delta\varepsilon$ = +26). The comparison to common carbohelicenes, which exhibit typical negative/positive ECD-active bands in solution[22] around 250 nm and 330 nm respectively,

allowed for the assignment of the absolute configuration of flavo[7]helicene enantiomers to (*P*) or (*M*)-helicity by directly reading their ECD fingerprint. The data obtained from measuring the circular dichroism of enantiomers of **1**@LCP confirmed that the prepared LCPs are optically active with chiroptical properties reflecting the original chirality of the loaded **1** enantiomers (**Figures 5E and 5F**).

Upon excitation at 520 nm, the enantiomers of compound **1** exhibited room temperature fluorescence at around 625 nm, with similar shapes in DCM and DMSO (**Figure 6**). Furthermore, pure enantiomers of **1** exhibited mirror-imaged circularly polarized luminescence (CPL), with a positive (negative) signal for the *P* (*M*) enantiomer, with $|g_{lum}|$ values of 4×10^{-3} at 625 nm. These values are typical for organic helicenes.[23] As expected, the enantiomers exhibit CPL signals with the same signs as those of the lowest-energy CD-active bands. In comparison, absorption dissymmetry factors were found to be higher ($|g_{abs}| = 7 \times 10^{-3}$ at 550 nm). Compound **1** exhibits quantum yields of 8.5 % in CH_2Cl_2 and 6 % in DMSO at room temperature. CP luminescence was observed exclusively in organic solvents and practically not at all in an aqueous environment. Details on its fluorescence quenching by water can be found in ref.[24]

Figure 6. (A) Emission and **(B)** CPL spectra of (*P*)-**1** (in red) and (*M*)-**1** (in blue). The measurements were performed in DCM (solid lines) or DMSO (dashed lines) for both panels.

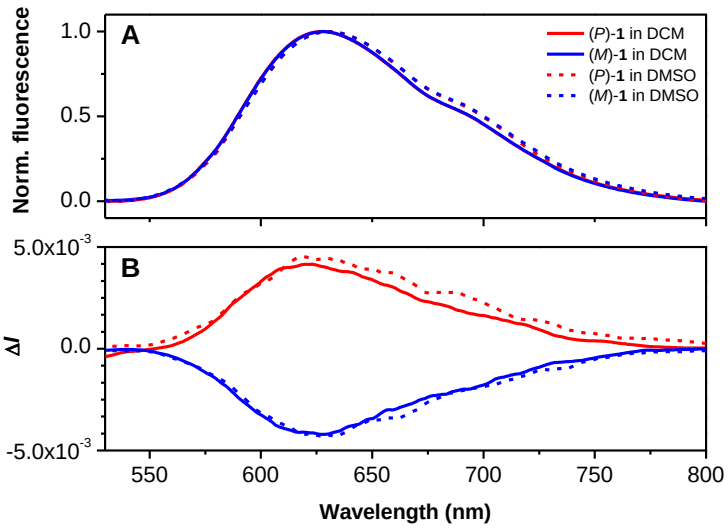

X-ray analysis. The identity of compound **1** was undoubtedly confirmed by X-ray crystallography. Suitable single crystals were obtained by crystallization from acetonitrile. The combination of flavin and helicene moieties impart novel structural features to molecule **1** that

are reflected in the molecular shape and also the molecular packing. Molecule **1** was compared to 3-methyllumiflavin (CCDC refcode MLUMIF)[25] and [7]helicene **2**[26] due to the similarity of some of their structural features to **1** (**Figure 7A**). In contrast to the molecule of flavin, all rings in **1** are significantly distorted from planarity. The distortion is mainly induced by steric hindrance of the inner N-CH_3 group pointing into the helicene cavity. It is even larger than in the corresponding rings in the carbohelicene analogue, as expressed by the total puckering amplitude (Q)[27] in **Figure 7A**. The introduction of the electron-withdrawing flavin part into the helicene skeleton leads to a contraction of the pitch between the rings due to electrostatic attraction compared to unsubstituted [7]helicene **2** (**Figure 7A**). The intermolecular interactions are also significantly affected by the presence of the flavin moiety. Compound **1** lost the ability to form homochiral domains, which results in lamellar twinning typical of carbohelicenes,[28] and crystallizes in the centrosymmetric space group $P2_1/c$. Additionally, a common motif found in the packing of carbohelicene molecules – a pair of interlocking molecules – is replaced by homochiral columnar structures along the Y axis (**Figure 7B**) where the flavin part interacts with helicene terminal rings of an adjacent molecule. The molecular columns are mutually linked by weak hydrogen bonding between the helicene periphery and flavin oxygen and nitrogen atoms (**Figures 7B and 7C**). This feature can also be found in the crystal packing of planar flavins, where it leads to the formation of two-dimensional molecular sheets that are mutually held in place by electrostatic interactions.[25]

CONCLUSIONS

In this study, flavin-helicene hybrid **1** was synthesized. Flavo[7]helicene **1** combines inherent helical chirality with redox activity, which was studied in solution (both aqueous and organic phases), in layers (electropolymers or films made of **1**@LCP), and in the solid state (a single crystal). In addition, a methodology that allows the loading of **1** enantiomers into an internally nanostructured lipid matrix (LCP) was developed, and it is one of the first examples of the incorporation of an inherently chiral molecule into transparent LCP material. Compound **1** embedded in the cubic phase film placed at the electrode surface reveals a quasi-reversible diffusion-controlled 2-electron redox process of the flavin headgroup. In addition, the lipophilic helicene parts of the molecule anchored in the lipidic bilayers of the cubic phase are less prone to oxidation at positive potentials which lead to polymer formation on the electrode for **1** dissolved in solution. The presented results could contribute to further research of other helicenes with switchable redox and optical properties with improved solubility in water. Furthermore, the loading of similar helicene-based hybrids into the hydrophobic lipidic matrix

(LCP) may find a wide spectrum of applications in analytical chemistry, (bio)sensing, and materials science in the future.

Figure 7. (**A**) ORTEP presentation of crystal structure of compound *rac*-**1** and its comparison to flavin and [7]helicene (**2**) molecule, all of them including puckering parameters Q, (**B**) the formation of columnar structures in the crystal packing of *rac*-**1**, and (**C**) hydrogen bonding between two molecules of *rac*-**1**.

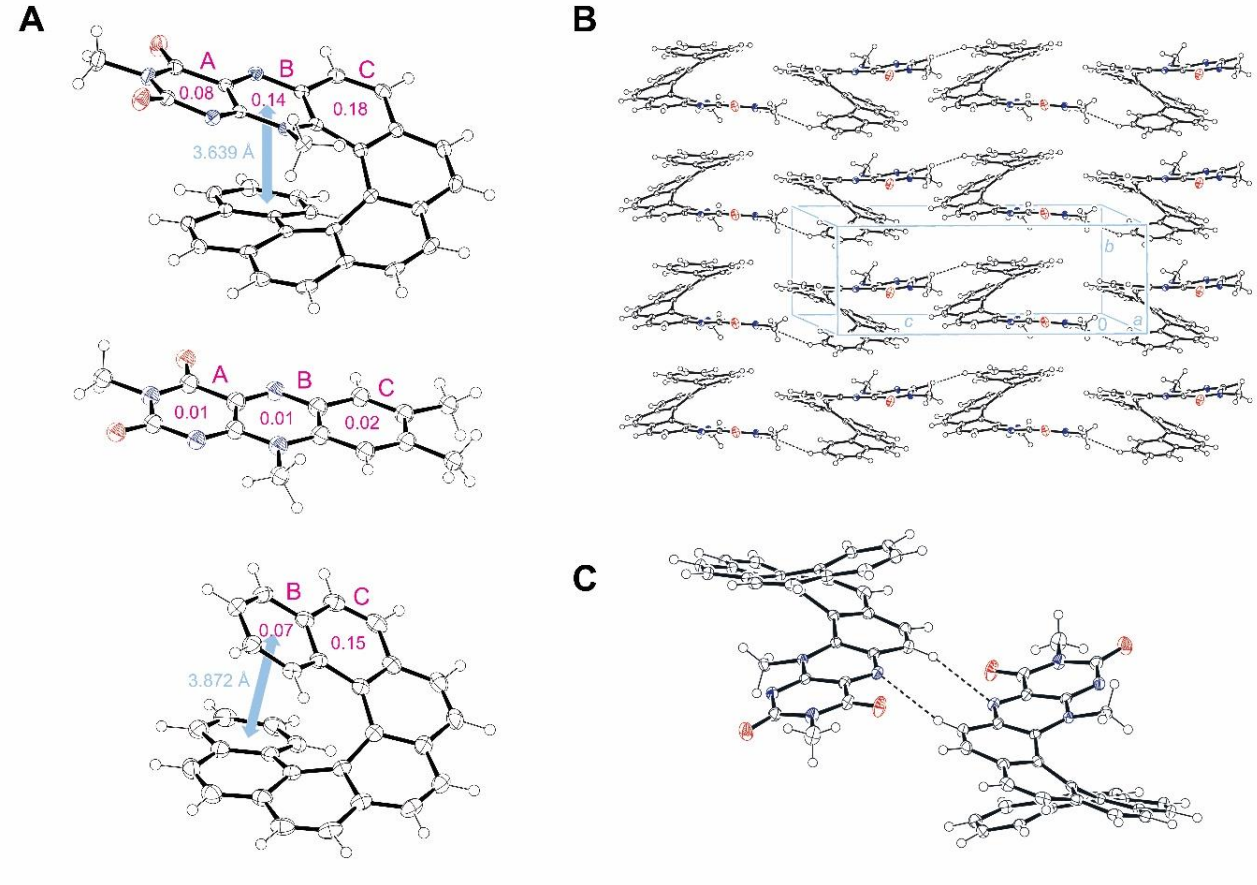

Acknowledgments

The authors are indebted to Dr. Jan Sykora (Institute of Chemical Process Fundamentals of the CAS) for structural analyses. The authors gratefully acknowledge the financial support of Palacky University, RVO 61989592 and internal grant IGA_LF_2020_022, from the Ministry of Education, Youth and Sports (MEYS, Czech Republic). This work was also partially supported by the Czech Science Foundation (grant no. 20-19353S). MEYS is also gratefully acknowledged for its support of international student exchanges, grant No. CZ.02.2.69/0.0/0.0/16_027/0008482. Computational resources were supplied by the project "e-Infrastruktura CZ" (No. e-INFRA LM2018140) provided within the program "Projects of Large Research, Development and Innovations Infrastructures".

EXPERIMENTAL

Chemicals and general methods

Commercially available reagent-grade materials were used as obtained from Sigma-Aldrich, and Fluorochem. 2-Nitroso[6]helicene was prepared according to a published procedure.[12] All solvents (Lach-Ner) were of reagent grade and used without any further purification, except for acetic acid, which was distilled from potassium permanganate. The standard Schlenk technique was used for all reactions. The melting point was determined with a Santiago KB T300 melting point apparatus (Czech Republic) and is uncorrected. TLC was performed on Silica gel 60 F_{254} or 60 RP-18 F_{254} aluminum sheets, and compounds were visualized with UV light (254 and 366 nm). Column chromatography was performed in an Isolera One system (Biotage) with pre-packed flash silica gel columns. Absorption spectra were recorded in a Specord 250 spectrometer (Jena Bioscience, Germany) in a quartz cuvette with a 1 cm optical path, using pure solvent as a reference. Steady-state excitation and emission spectra were recorded using an F-4500 fluorometer (Hitachi, Japan) in a quartz cuvette with a 1 cm optical path (for both excitation and emission). The IR spectra were measured in $CHCl_3$ (Nicolet 6700). Characteristic IR absorptions are reported in cm^{-1} and denoted as strong (s), medium (m), or weak (w). The circular dichroism (CD) spectra (in $M^{-1}cm^{-1}$) were recorded in a J-815 spectrometer (Jasco Analytical Instruments, Inc., Easton, PA) at the IFR140 facility (Biosit platform - Université de Rennes 1). Circularly polarized luminescence (CPL) measurements were performed using a home-built CPL spectrofluoropolarimeter (with the help of the company JASCO). The samples were excited using 90° geometry with a 150 W LS ozone-free Xenon lamp. The spectra were measured in 10^{-5} M CH_2Cl_2 or DMSO solutions in a 1 cm cell under deoxygenated conditions. The solutions were degassed by at least 3 freeze/pump/thaw cycles in a sealed transparent glass apparatus that included the measuring cell whilst being connected to the vacuum manifold. The parameters were: emission bandwidth ~ 1.0 nm, integration time = 4 sec, scan speed = 50 nm/min, accumulations = 10. ^1H and $^{13}C\{^1H\}$ spectra were recorded using a Bruker Avance 400 and a Varian Inova 500 MHz instrument. Chemical shifts (δ) are reported in parts per million (ppm) relative to TMS or referenced to residuals of $CDCl_3$ or d^7-DMF (δ = 7.26 ppm and δ = 77.00 ppm, respectively for *d*-chloroform and δ = 2.92 ppm for d^7-DMF). The coupling constants *J* are given in Hz. COSY, HSQC, and HMBC experiments were performed to correctly assign both the ^1H and ^{13}C NMR spectra of compound **1**. For precise mass measurement, the spectra were internally calibrated using Na-formate or APCI-TOF tuning mix. ESI and APCI high-resolution mass spectra were measured in positive mode using a

micrOTOF QIII mass spectrometer (Bruker), and were determined with the software Compass Data Analysis. Diffraction data were collected in a Bruker D8 VENTURE Kappa Duo PHOTON 100 CMOS with monochromated Mo/Cu−Kα radiation. The structures were solved by direct methods (SHELXT[29]) and refined by full-matrix least-squares on F^2 values (CRYSTALS[30] or SHELXL[29]). All heavy atoms were refined anisotropically. Hydrogen atoms were localized from the expected geometry and difference electron density maps, and were refined isotropically. ORTEP-3 was used for structure presentation.[31] The crystallographic data for the structures reported in this paper have been deposited with the Cambridge Crystallographic Data Centre as a supplementary publication. Copies of the data can be obtained free of charge by applying to the CCDC. The resolution of enantiomers of **1** was performed by semi-preparative HPLC with a UV detector at 320 nm (Watrex) using a chiral stationary phase Chiralpak IB® (Diacel) column (250 × 20 mm, 10 µm) and *n*-heptane/2-propanol 70:30 + 5 %vol. DCM + 0.5 %vol. The mobile phase was NEt_2H at a flow rate of 12 mL min^{-1}. The optical purity of each enantiomer of **1** was checked by the integration of UV traces (254 nm) of HPLC chromatograms at the Varian ProStar 230 SDA + ProStar 330 PDA detector (200–400 nm). The HPLC analyses were performed in a Chiralpak IB® (Diacel) column (250 × 4.6 mm, 10 µm) using *n*-heptane/2-propanol 70:30 + 0.5 %vol. The mobile phase was NEt_2H at a flow rate of 2 mL min^{-1}. The same instrument was used for the determination of %ee values for the oxidative kinetic resolution of 1-(4-methoxyphenyl)ethanol. The HPLC analyses were performed acc. to ref.[32] in a Chiralcel® OD-H (Chiral Technologies) column (150 × 4.6 mm, 5 µm) using *n*-hexane/ethanol 97:3 as the mobile phase at a flow rate of 1 mL min^{-1}. Specific optical rotations ($[\alpha]_D^{20}$) were measured at 589 nm in chloroform at 20 °C in a JASCO P-2000 polarimeter with a Peltier cell holder and a 1 dm path length cell. The values are given in deg cm^3 g^{-1} dm^{-1} as an average value from 50 measurements. The SAXS experiments were carried out with a Bruker Nanostar system equipped with a Vantec-2000 area detector using CuKα radiation (λ = 1.54 Å). LCP samples were injected into 1.5-mm diameter quartz capillaries sealed with epoxy glue (UHU). All electrochemical measurements in an aqueous environment and LCP were performed at room temperature with an Autolab and a three-electrode arrangement with an Ag/AgCl/3M KCl electrode as the reference and platinum foil as the auxiliary electrode. Cyclic voltammetry (CV) experiments were carried out using a GCE (BASi, 3 mm diameter, or GCE, Bio-Logic SAS, 1 mm diameter). Electrochemistry in a non-aqueous environment of ACN and DCM was performed using a Nanoampere electrochemical workstation (L-Chem, CZ) in three-electrode configuration with a BASi, 3 mm diameter GC, LF2 (Innovative Instruments) leak-free

reference electrode, and platinum wire auxiliary electrode. The working solutions were deaerated using an argon stream presaturated with a given solvent. After the measurement, the potentials were rescaled against ferrocene/ferrocenium midpoint potentials obtained from separate CV experiments.

Synthesis of flavo[7]helicene 1

The preparation of compound **1** (15,18-dimethyl-15*H*-[6]heliceno[2,1-*g*]pteridin-17,19-dione) was performed as follows: 2-nitroso[6]helicene (100 mg, 0.28 mmol) and 3-methyl-6-(methylamino)uracil (130 mg, 0.84 mmol, 3 eq) were placed in an oven-dried Schlenk flask under an argon atmosphere. Degassed glacial acetic acid (20 ml) was added, and the reaction was heated to 100 °C overnight. After the reaction was complete (observed by TLC), the solvent was evaporated and the solid residue was chromatographed on silica gel with ethyl acetate as the mobile phase. The product **1** was obtained as a purple solid (44 mg, 32 % yield). **mp:** 216 – 217 °C (acetonitrile). **^{1}H NMR (500 MHz, $CDCl_3$)**: 2.25 (3H, s), 3.55 (3H, s), 6.53 (1H, t, *J* = 7.71 Hz), 6.93 (1H, d, *J* = 8.5 Hz), 7.16 (1H, t, *J* = 7.4 Hz), 7.43 (2H, t, *J* = 7.7 Hz), 7.75 - 7.81 (2H, m), 7.92 (1H, d, *J* = 8.5 Hz), 7.97 - 8.05 (3H, m), 8.11 (1H, d, *J* = 8.2 Hz), 8.15 (1H, d, *J* = 8.2 Hz), 8.24 (1H, d, *J* = 8.2 Hz) ppm. **^{13}C NMR (126 MHz, $CDCl_3$)**: 28.71 (s), 40.30 (s), 118.35 (s), 123.27 (s), 124.25 (s), 124.51 (s), 125.07 (s), 126.07 (s), 126.34 (s), 126.46 (s), 126.65 (s), 126.73 (s), 126.79 (s), 126.86 (s), 127.14 (s), 127.22 (s), 127.55 (s), 127.93 (s), 128.64 (s), 129.24 (s), 130.86 (s), 131.80 (s), 132.17 (s), 132.46 (s), 132.73 (s), 133.65 (s), 134.54 (s), 136.59 (s), 136.99 (s), 148.17 (s), 156.10 (s), 159.67 (s) ppm. **IR** ($CHCl_3$) cm^{-1}: 3047 w, 1704 m, 1658 s, 1609 m, 1553 vs, 1542 vs, 1505 m, 1459 w, 1425 m, 1416 m, 1378 vw, 1278 m, 1260 m, 1227 m, 1157 m, 969 w, 869 w, 848 m, 747 m, 599 w, 418 w. **HR ESI MS:** calculated for **[**$C_{32}H_{20}N_4O_2$+H]$^+$ 493.1664, found 493.1654. **Chiral resolution:** t_R = 33 min for (*M*)**-1** and 42 min for (*P*)**-1** in prep. mode. **Optical rotation:** $[\alpha]_D^{20}$ = +2246° (c = 0.052, chloroform) for dextrorotatory (*P*)**-1** and $[\alpha]^{20}_D$ = −2306° (c = 0.046, chloroform) for levorotatory (*M*)**-1**. **X-ray** data of compound **1**: $C_{32}H_{20}N_4O_2$, *M* = 492.54 g/mol, monoclinic system, space group $P2_1/c$, *a* = 15.5546(5), *b* = 7.1648(2), *c* = 20.3719(6) Å, β = 100.338(1)°, *Z* = 4, *V* = 2233.50(12) Å^3, *D*c = 1.46 g.cm^{-3}, μ(Cu Kα) = 0.75 mm^{-1}, *T* = 120 K, crystal dimensions of 0.09 × 0.17 × 0.33 mm. The structure converged to a final *R* = 0.0342 and R_w = 0.0858 using 4289 independent reflections for 423 refined parameters (θ_{max} = 72.15°). CCDC No. 2061539.

Synthesis of Dihydroflavo[7]helicene (1-H_2)

Flavo[7]helicene **1** (10 mg, 0.02 mmol) and Pd/C (10 wt%, 5 mg) was charged into a Schlenk flask, purged with argon, and dissolved in d^7-DMF (3 ml). Then, a balloon containing hydrogen gas was attached and the reaction flask was flushed with hydrogen several times. The reaction mixture was then stirred for approximately 3 hours at room temperature until the color changed from magenta to yellow-brown. The stirring was then stopped and the dispersed palladium was allowed to settle down at the bottom of the flask. A small sample of the reaction mixture was transferred *via* syringe to an argon-flushed NMR cuvette, however rapid change back to a magenta-colored solution was observed within seconds. The subsequent ^{1}H NMR measurement showed approximately 30% conversion to **1-H_2** (for spectra, see Supporting Information). This partially reduced solution fully reoxidized to **1** alone within minutes.

Preparation of monoolein-based LCP

Cubic phases without enantiomers were prepared by mixing the appropriate amount of molten 1-monoolein (MO) and water at room temperature in small glass vials. The ratio of components was chosen based on the phase diagram for the MO/water system.[33] The composition of the non-doped LCPs was 60/40 (%, *w*/*w*) for MO/water. (*P*)/(*M*)-**1**@LCPs were prepared as follows. The enantiomers were dissolved in the molten MO and mixed with an appropriate amount of water at room temperature. The final composition of the LCPs was 59.8/0.2/40 (%, *w*/*w*) for MO/**1** enantiomer/water. Samples were stabilized for at least 24 h to obtain transparent, viscous, and homogenous LCPs. Samples were stored in tightly closed vials at room temperature in the dark. Their stability was confirmed by microscopic observation of the samples and by small-angle X-ray scattering (SAXS) measurements. The determination of experimental SAXS parameters is described in the Supporting Information.

Preparation of helicene-based polymers on ITO electrodes

A stock solution of (*M*)-enantiomer of compound **1** was dissolved in DMSO to a concentration of 1 mg/ml and then diluted to 50 µM in Britton-Robinson buffer at pH 7.4. The ITO electrode was electrodeposited with 50 µM (*M*)-**1** at +1.5 V for 120 s in Britton-Robinson buffer (pH 7.4), which was not deoxygenated.

REFERENCES

[1] a) M. Gingras, *Chem. Soc. Rev.* **2013**, *42*, 1051-1095; b) M. Gingras, *Chem. Soc. Rev.* **2013**, *42*, 968-1006; c) M. Gingras, G. Felix and R. Peresutti, *Chem. Soc. Rev.* **2013**, *42*, 1007-1050.
[2] a) J. E. Field, G. Muller, J. P. Riehl and D. Venkataraman, *J. Am. Chem. Soc.* **2003**, *125*, 11808-11809; b) D. J. Morrison, T. K. Trefz, W. E. Piers, R. McDonald and M. Parvez, *J. Org. Chem.* **2005**, *70*, 5309-5312; c) Y. Ooyama, G. Ito, H. Fukuoka, T. Nagano, Y. Kagawa, I. Imae, K. Komaguchi and Y. Harima, *Tetrahedron* **2010**, *66*, 7268-7271; d) Y. Tang, T. A. Cook and A. E. Cohen, *J. Phys. Chem. A* **2009**, *113*, 6213-6216.
[3] a) T. Hatakeyama, S. Hashimoto, T. Oba and M. Nakamura, *J. Am. Chem. Soc.* **2012**, *134*, 19600-19603; b) Y. Yang, R. C. Da Costa, M. J. Fuchter and A. J. Campbell, *Nat. Photonics* **2013**, *7*, 634-638.
[4] a) L. Shi, Z. Liu, G. Dong, L. Duan, Y. Qiu, J. Jia, W. Guo, D. Zhao, D. Cui and X. Tao, *Chem. Eur. J.* **2012**, *18*, 8092-8099; b) J. Storch, J. Zadny, T. Strasak, M. Kubala, J. Sykora, M. Dusek, V. Cirkva, P. Matejka, M. Krbal and J. Vacek, *Chem. Eur. J.* **2015**, *21*, 2343-2347; c) J. Vacek, J. Zadny, J. Storch and J. Hrbac, *ChemPlusChem* **2020**, *85*, 1954–1958.
[5] C.-F. Chen and Y. Shen, *Helicene Chemistry: From Synthesis to Applications. Springer, Heidelberg* **2016**.
[6] M. Jakubec and J. Storch, *J. Org. Chem.* **2020**, *85*, 13415–13428.
[7] K. Watanabe, K. Suda and K. Akagi, *J. Mat. Chem. C* **2013**, *1*, 2797-2805.
[8] K. Dhbaibi, L. Favereau and J. Crassous, *Chem. Rev.* **2019**, *119*, 8846-8953.
[9] M. Jakubec, S. Hansen-Trooyen, I. Cisarova, J. Sykora and J. Storch, *Org. Lett.* **2020**, *22*, 3905-3910.
[10] a) R. Cibulka, *Eur. J. Org. Chem.* **2015**, *2015*, 915-932; b) A. M. Edwards in *Structure and general properties of flavins*, *Vol. 1146* **2014**, pp. 3-13; c) H. Iida, Y. Imada and S. I. Murahashi, *Org. Biomol. Chem.* **2015**, *13*, 7599-7613; d) B. König, S. Kümmel, E. Svobodova and R. Cibulka, *Phys. Sci. Rev. (10.1515/psr-2017-0168)* **2018**, *3*; e) V. Massey, *Biochem. Soc. Trans.* **2000**, *28*, 283-296.
[11] E. M. Seward, R. Bruce Hopkins, W. Sauerer, S. W. Tam and F. Diederich, *J. Am. Chem. Soc.* **1990**, *112*, 1783-1790.
[12] M. Jakubec, T. Beranek, P. Jakubik, J. Sykora, J. Zadny, V. Cirkva and J. Storch, *J. Org. Chem.* **2018**, *83*, 3607-3616.
[13] a) E. M. Landau and J. P. Rosenbusch, *Proc. Natl. Acad. Sci. U.S.A.* **1996**, *93*, 14532-14535; b) E. Nazaruk, R. Bilewicz, G. Lindblom and B. Lindholm-Sethson, *Anal. Bioanal. Chem.* **2008**, *391*, 1569-1578; c) M. Zatloukalova, E. Nazaruk, D. Novak, J. Vacek and R. Bilewicz, *Biosens. Bioelectron.* **2018**, *100*, 437-444.
[14] a) M. Caffrey and V. Cherezov, *Nature Prot.* **2009**, *4*, 706-731; b) D. Li and M. Caffrey, *Proc. Natl. Acad. Sci. U.S.A.* **2011**, *108*, 8639-8644; c) M. Maeki, H. Yamaguchi, M. Tokeshi and M. Miyazaki, *Anal. Sci.* **2016**, *32*, 3-9; d) E. Nazaruk, E. Górecka, Y. M. Osornio, E. M. Landau and R. Bilewicz, *J. Electroanal. Chem.* **2018**, *819*, 269-274.
[15] C. V. Kulkarni, W. Wachter, G. Iglesias-Salto, S. Engelskirchen and S. Ahualli, *Phys. Chem. Chem. Phys.* **2011**, *13*, 3004-3021.
[16] a) J. J. Hasford and C. J. Rizzo, *J. Am. Chem. Soc.* **1998**, *120*, 2251-2255; b) H. Tatsumi, H. Nakase, K. Kano and T. Ikeda, *J. Electroanal. Chem.* **1998**, *443*, 236-242.
[17] J. Hrbac, V. Pavelka, J. Crassous, J. Zadny, L. Fekete, J. Pokorny, P. Vanysek, J. Storch and J. Vacek, *Electrochem. Commun.* **2020**, *113*, 106689.
[18] A. J. Bard and L. R. Faulkner, *Electrochemical methods: fundamentals and applications, John Willey & Sons, New York, USA* **2001**.
[19] Y.-M. Legrand, M. Gray, G. Cooke and V. M. Rotello, *J. Am. Chem. Soc.* **2003**, *125*, 15789-15795.

[20] a) E. Nazaruk, P. Miszta, S. Filipek, E. Górecka, E. M. Landau and R. Bilewicz, *Langmuir* **2015**, *31*, 12753-12761; b) P. Rowiński, A. Korytkowska and R. Bilewicz, *Chem. Phys. Lipids* **2003**, *124*, 147-156.
[21] a) M. Ben Braiek, F. Aloui, S. Moussa and B. Ben Hassine, *Tetrahedron Lett.* **2015**, *56*, 6580-6584; b) M. J. Fuchter, M. Weimar, X. Yang, D. K. Judge and A. J. P. White, *Tetrahedron Lett.* **2012**, *53*, 1108-1111.
[22] J. Storch, K. Kalíková, E. Tesařová, V. Maier and J. Vacek, *J. Chromatogr. A* **2016**, *1476*, 130-134.
[23] a) J. Crassous, *Circularly Polarized Luminescence of Isolated Small Organic Molecules, T. Mori (ed.), Springer, chap. 4, pp 53-97* **2020**; b) W.-L. Zhao, M. Li, H.-Y. Lu and C.-F. Chen, *Chem. Commun.* **2019**, *55*, 13793-13803.
[24] G. E. Dobretsov, T. I. Syrejschikova and N. V. Smolina, *Biophysics (Russian Federation)* **2014**, *59*, 183-188.
[25] R. Norrestam and B. Stensland, *Acta Crys. Sec. B* **1972**, *28*, 440-447.
[26] J. Sykora, I. Cisarova, V. Cirkva and J. Stroch, *CCDC 2061539: Experimental Crystal Structure Determination, DOI: 10.5517/ccdc.csd.cc27668y* **2021**.
[27] D. Cremer and J. A. Pople, *J. Am. Chem. Soc.* **1975**, *97*, 1354-1358.
[28] B. S. Green and M. Knossow, *Science* **1981**, *214*, 795-797.
[29] G. M. Sheldrick, *Acta Crystallogr. Sect. A* **2015**, *71*, 3-8.
[30] P. W. Betteridge, J. R. Carruthers, R. I. Cooper, K. Prout and D. J. Watkin, *J. Appl. Crystallogr.* **2003**, *36*, 1487.
[31] L. Farrugia, *J. Appl. Crystallogr.* **1997**, *30*, 565.
[32] E. M. Ferreira and B. M. Stoltz, *J. Am. Chem. Soc.* **2001**, *123*, 7725-7726.
[33] H. Qiu and M. Caffrey, *Biomaterials* **2000**, *21*, 223-234.